

A Lagrangian particle/panel method for the barotropic vorticity equations on a rotating sphere

Peter Bosler¹, Lei Wang², Christiane Jablonowski³ and Robert Krasny¹‡

¹Department of Mathematics, University of Michigan, Ann Arbor, MI 48109, USA

²Department of Mathematical Sciences, University of Wisconsin-Milwaukee, Milwaukee, WI 53201, USA

³Department of Atmospheric, Oceanic, and Space Sciences, University of Michigan, Ann Arbor, MI 48109, USA

E-mail: krasny@umich.edu

Abstract. We present a Lagrangian particle/panel method for geophysical fluid flow described by the barotropic vorticity equations on a rotating sphere. The particles carry vorticity and the panels are used in discretizing the Biot-Savart integral for the velocity. Adaptive panel refinement and a new Lagrangian remeshing scheme are applied to reduce the computational cost and maintain accuracy as the flow evolves. Computed examples include a Rossby-Haurwitz wave, a Gaussian vortex, and a perturbed zonal jet. To validate the method, a comparison is made with results obtained using the Lin-Rood finite-volume scheme.

Keywords: Barotropic vorticity equations, Flow map, Lagrangian particle/panel method, Point vortex approximation, Adaptive refinement, Remeshing

1. Introduction

There is continuing interest in improving the numerical methods used in geophysical fluid flow simulations (Behrens 2006). Current approaches include finite-volume methods (Lin and Rood 1996) and spectral element methods (Taylor and Fournier 2010), but the complex dynamics in these flows is still challenging and it is worthwhile to investigate alternative methods. As a step in that direction we present a Lagrangian particle/panel method (LPPM) for the barotropic vorticity equations on a rotating sphere (Bosler 2013, Wang 2010). In this method, the particles carry vorticity and the panels are used in discretizing the Biot-Savart integral for the velocity. A number of previous studies of vortex dynamics on a sphere have dealt with point vortices, vortex patches, and vortex sheets (e.g. Dritschel 1988, Kidambi and Newton 1998, Surana and Crowley 2008, Sakajo 2009, Kropinski and Nigam 2013), but the present work is concerned with general smooth vorticity distributions.

In many Lagrangian particle simulations of fluid flow the particles initially lie on a regular grid, but they typically become disordered and the numerical error increases in time (Perlman 1985). Previous investigators addressed this problem with remeshing and refinement schemes (e.g. Russo and Strain 1994, Koumoutsakos 1997, Barba *et al* 2005), and we follow the same approach here, although the specific techniques we use are different. In particular, we use an adaptive panel refinement scheme motivated by prior work on vortex sheets (Feng *et al* 2009) and a new Lagrangian remeshing scheme that avoids directly interpolating the vorticity (Bosler 2013). We use the point vortex approximation to discretize the Biot-Savart integral and rely on the refinement and remeshing schemes to maintain the accuracy of this approach. We note that several other Lagrangian methods have been developed for geophysical fluid flow (e.g. Dritschel *et al* 1999, Alam and Lin 2008).

First we present the Eulerian form of the barotropic vorticity equations (BVE) on a rotating sphere, then the Green’s function based solution of the Poisson equation, then the Lagrangian form of the BVE, followed by the discretization, the remeshing and refinement schemes, numerical results, discussion, and finally conclusions. A preliminary account of this work was presented at the IUTAM Symposium on “Vortex Dynamics: Formation, Structure and Function”, March 10-14, 2013, Fukuoka, Japan.

2. Eulerian form

All quantities are dimensionless except as noted. Our presentation follows Vallis (2006). Let S denote the unit sphere representing the Earth with rotation rate Ω about the z -axis. For the case of incompressible flow considered here, the fluid velocity $\mathbf{u}(\mathbf{x}, t)$ is related to the stream function $\psi(\mathbf{x}, t)$ by

$$\mathbf{u} = \nabla\psi \times \mathbf{x}, \tag{1}$$

where $\mathbf{x} \in S$ is a point on the sphere. The stream function and relative vorticity $\zeta(\mathbf{x}, t)$ satisfy the Poisson equation,

$$\Delta\psi = -\zeta, \quad (2)$$

where the operator on the left is the spherical Laplacian or Laplace-Beltrami operator. Finally, we have the conservation of absolute vorticity,

$$\frac{D(\zeta + f)}{Dt} = \frac{\partial(\zeta + f)}{\partial t} + \mathbf{u} \cdot \nabla(\zeta + f) = 0, \quad (3)$$

where D/Dt is the material derivative and $f = 2\Omega z$ is the Coriolis parameter. With an initial relative vorticity, $\zeta(\mathbf{x}, 0) = \zeta_0(\mathbf{x})$, these equations comprise the Eulerian form of the BVE on a rotating sphere.

3. Poisson equation

Many numerical methods are available for solution of the Poisson equation (2) including finite-difference, finite-element, and spectral methods. However following Bogomolov (1977) and Kimura and Okamoto (1987), we employ the spherical Green's function,

$$g(\mathbf{x}, \mathbf{y}) = -\frac{1}{4\pi} \log(1 - \mathbf{x} \cdot \mathbf{y}), \quad \mathbf{x}, \mathbf{y} \in S, \quad (4)$$

from which the stream function is obtained by convolution with the vorticity,

$$\psi(\mathbf{x}, t) = \int_S g(\mathbf{x}, \mathbf{y}) \zeta(\mathbf{y}, t) dS(\mathbf{y}). \quad (5)$$

Applying (1) to (5) yields the velocity as a spherical Biot-Savart integral,

$$\mathbf{u}(\mathbf{x}, t) = -\frac{1}{4\pi} \int_S \frac{\mathbf{x} \times \mathbf{y}}{1 - \mathbf{x} \cdot \mathbf{y}} \zeta(\mathbf{y}, t) dS(\mathbf{y}). \quad (6)$$

4. Lagrangian form

We follow the approach used in deriving the vortex method for incompressible fluid flow in Euclidean space (Chorin and Marsden 1979, Cottet and Koumoutsakos 2000). The Lagrangian form of the BVE is based on the flow map. For a given velocity field $\mathbf{u}(\mathbf{x}, t)$, the flow map $\mathbf{x}(\mathbf{a}, t)$ is defined by the equations

$$\frac{\partial \mathbf{x}}{\partial t}(\mathbf{a}, t) = \mathbf{u}(\mathbf{x}(\mathbf{a}, t), t), \quad \mathbf{x}(\mathbf{a}, 0) = \mathbf{a}, \quad (7)$$

where $\mathbf{a} \in S$ is a Lagrangian parameter. Hence the flow map gives the current location of the fluid particle which was initially located at \mathbf{a} .

Next, substituting (6) into (7), changing variables using the flow map $\mathbf{y} = \mathbf{x}(\mathbf{b}, t)$, and noting that the Jacobian determinant is unity for incompressible flow, we obtain

$$\frac{\partial \mathbf{x}}{\partial t}(\mathbf{a}, t) = -\frac{1}{4\pi} \int_S \frac{\mathbf{x}(\mathbf{a}, t) \times \mathbf{x}(\mathbf{b}, t)}{1 - \mathbf{x}(\mathbf{a}, t) \cdot \mathbf{x}(\mathbf{b}, t)} \zeta(\mathbf{x}(\mathbf{b}, t), t) dS(\mathbf{b}). \quad (8)$$

The conservation of absolute vorticity (3) is expressed as

$$\frac{D\zeta}{Dt}(\mathbf{x}(\mathbf{a}, t), t) = -2\Omega \frac{\partial z}{\partial t}(\mathbf{a}, t), \quad \zeta(\mathbf{a}, 0) = \zeta_0(\mathbf{a}). \quad (9)$$

Equations (8)-(9) are a coupled system of evolution equations for the flow map and relative vorticity, and this is the desired Lagrangian form of the BVE on a rotating sphere. The advection of a passive tracer is given by the equation

$$\phi(\mathbf{x}(\mathbf{a}, t), t) = \phi(\mathbf{a}, 0). \quad (10)$$

5. Discretization

The flow map is discretized using a particle/panel method as in recent three-dimensional vortex sheet computations (Feng *et al* 2009). The sphere is expressed as a set of panels,

$$S = \cup_{k=1}^N A_k, \quad (11)$$

where each panel A_k defines a region in the spherical Lagrangian parameter space. We consider two types of panels shown in figure 1, (a) icosahedral triangles, and (b) cubed-sphere quadrilaterals.

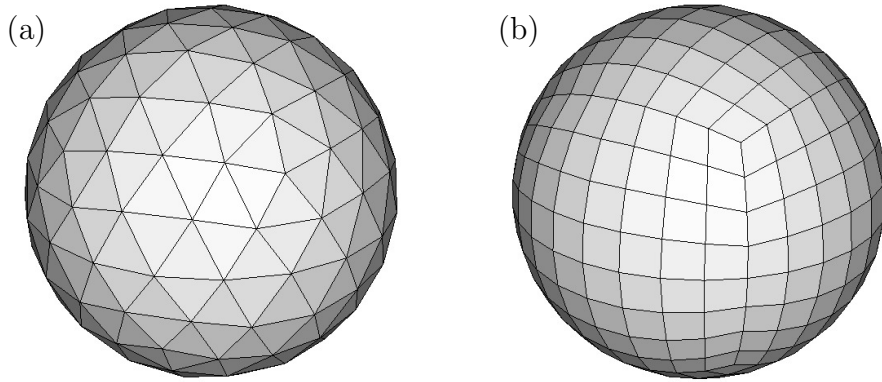


Figure 1. Panel discretization of sphere, (a) icosahedral triangles, (b) cubed-sphere quadrilaterals.

In addition, as shown in figure 2 each panel has associated particles, an active particle $\mathbf{x}_j(t) \approx \mathbf{x}(\mathbf{a}_j, t)$, $j = 1 : N$ at the center and passive particles $\mathbf{y}_i(t) \approx \mathbf{y}(\mathbf{a}_i, t)$, $i = 1 : M$ at the vertices. The particles carry vorticity, $\zeta_{i,j}(t) \approx \zeta(\mathbf{x}(\mathbf{a}_{i,j}), t)$, associated with a Lagrangian parameter value. The particles are advected in the flow; the active particles contribute their vorticity to the Biot-Savart integral, and the passive particles define the panel domains.

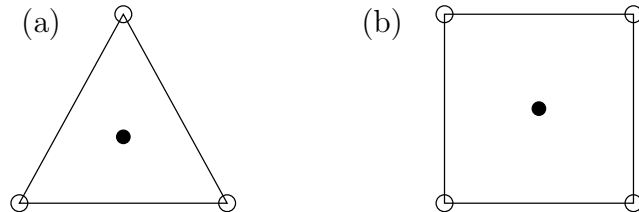


Figure 2. Panels, (a) triangle, (b) quadrilateral; each panel has an active particle at the center (•), and passive particles at the vertices (◦).

The Biot-Savart integral in (8) is discretized by the midpoint rule, and then combined with the conservation of absolute vorticity (9), we obtain a set of ordinary differential equations,

$$\frac{d\mathbf{x}_j}{dt} = -\frac{1}{4\pi} \sum_{\substack{k=1 \\ k \neq j}}^N \frac{\mathbf{x}_j \times \mathbf{x}_k}{1 - \mathbf{x}_j \cdot \mathbf{x}_k} \zeta_k A_k, \quad j = 1 : N, \quad (12)$$

$$\frac{d\mathbf{y}_i}{dt} = -\frac{1}{4\pi} \sum_{k=1}^N \frac{\mathbf{y}_i \times \mathbf{x}_k}{1 - \mathbf{y}_i \cdot \mathbf{x}_k} \zeta_k A_k, \quad i = 1 : M, \quad (13)$$

$$\frac{d\zeta_{i,j}}{dt} = -2\Omega \frac{dz_{i,j}}{dt}, \quad (14)$$

where A_k is the spherical area of panel k which is invariant in time due to incompressibility. Note that the singular term $k = j$ in (12) is omitted; hence these equations describe a system of point vortices on a rotating sphere. Previous work has investigated point vortex dynamics on a sphere (Newton 2001), but here the system (12)-(14) arises by discretizing the Lagrangian form of the BVE and we are concerned with convergence to a smooth vorticity distribution as the number of points becomes large.

The initial conditions are treated as follows. The initial particle positions $\mathbf{a}_{i,j}$ are determined by the choice of the Lagrangian mesh, i.e. icosahedral triangles or cubed-sphere quadrilaterals. The initial particle vorticity is obtained from a given distribution, $\zeta_{i,j}(0) = \zeta_0(\mathbf{a}_{i,j})$. Following (10), each particle also has a passive tracer value which is a material invariant, $\phi_{i,j}(t) = \phi_0(\mathbf{a}_{i,j})$. In this work the passive tracer is chosen to be the latitude of the initial particle position.

The ODEs (12)-(14) are solved by the 4th order Runge-Kutta method. The particle positions are expressed in Cartesian coordinates; this avoids the pole singularities present in spherical coordinates and will facilitate extension to three-dimensional flows in future work. Hence the particles are not constrained to lie on the sphere, but in practice they remain close to the sphere as long as the flow is well-resolved.

The code was written in Fortran90/95. Several data structures keep track of the particles and panels. The 3D spherical plots were made with the Visualization Toolkit (VTK) and 2D contour plots were done with the NCAR Command Language (NCL). Most of the computations were done on a Mac desktop (3.4 GHz Intel Core i7, 16 GB RAM). One computation with a large number of panels, $N = 81920$, was done in parallel on the University of Michigan Flux cluster (Intel Core i7 Nehalem, 12 cores per node, 48 GB RAM per node). The parallel computation used MPI and a replicated data approach to evaluate the sums in (12)-(13), and required 5.8 hr of cpu time on 48 cores.

6. Numerical results

Results are presented for three examples, a Rossby-Haurwitz wave, a Gaussian vortex, and a perturbed zonal jet. In all cases the sphere rotation rate is $\Omega = 2\pi$. The initial vorticity is expressed in terms of longitude λ and latitude θ , where $\mathbf{x} = (x, y, z)^T = (\cos \lambda \cos \theta, \sin \lambda \cos \theta, \sin \theta)^T$.

6.1. Rossby-Haurwitz wave

The first example is a Rossby-Haurwitz (RH) wave for which the stream function is a spherical harmonic with zonal wavenumber $m = 4$. The initial vorticity is

$$\zeta_0(\lambda, \theta) = \frac{2\pi}{7} \sin \theta + 30 \sin \theta \cos^4 \theta \cos 4\lambda. \quad (15)$$

The RH wave propagates with constant speed and the first term on the right puts the wave into a steady reference frame so that (15) is also the vorticity for $t > 0$.

Figure 3 displays the results with $N = 5120$ triangles and time step $\Delta t = 0.01$, showing the vorticity (left), panels (middle), and passive tracer (right). Two times are shown, $t = 0$ (top), and $t = 1$ (middle, bottom) corresponding to one revolution of the sphere. In the vorticity plots, red indicates positive values (counterclockwise rotation) and blue indicates negative values (clockwise rotation). As noted above, the vorticity is visualized in a steady frame and is invariant in time; however the fluid velocity is nonzero, implying that the particles follow time-dependent trajectories, and the passive tracer is advected in the flow. From the results in figure 3 (top) we see that the solution is initially well-resolved, but figure 3 (middle) shows that the particle/panel distribution becomes disordered later in time and this leads to large errors in the vorticity and passive tracer. This is typical for Lagrangian particle simulations (Perlman 1985).

6.2. Remeshing

Remeshing is often used in particle simulations to restore the particle order and maintain accuracy. One approach interpolates the vorticity from the current particles \mathbf{x}_j to a new set of particles \mathbf{x}_j^n lying on a regular grid (e.g. Koumoutsakos 1997). Here we employ a new Lagrangian remeshing scheme that avoids directly interpolating the vorticity (Bosler 2013). The scheme constructs a Delaunay triangulation of the current particles \mathbf{x}_j , and the new particles \mathbf{x}_j^n lying on a regular grid are located within the triangulation. Then the corresponding new Lagrangian parameter values \mathbf{a}_j^n are computed by inverse interpolation of the flow map, $\mathbf{x}_j^n = \hat{\mathbf{x}}(\mathbf{a}_j^n, t)$, where $\hat{\mathbf{x}}(\mathbf{a}, t)$ is a discrete approximation based on the Delaunay triangulation. The vorticity of the new particles is then evaluated by sampling the initial vorticity at the new Lagrangian parameter values, $\zeta_j^n = \zeta_0(\mathbf{a}_j^n) + f(\mathbf{a}_j^n) - f(\mathbf{x}_j^n)$, using the conservation of absolute vorticity. This scheme was implemented using the Delaunay triangulation and cubic Hermite interpolation routines from the SSRFPACK library (Renka 1997a, 1997b).

The results in figure 3 (bottom) were obtained by applying this Lagrangian remeshing scheme every 10 time steps. The computed vorticity at $t = 1$ is now very close to the initial vorticity, showing that the scheme succeeds in maintaining accuracy. We see that passive tracer material from the poles has rolled up smoothly around each vortex core. At present the number of time steps between remeshing operations is determined empirically and intervals of 10-20 time steps are used in this work.

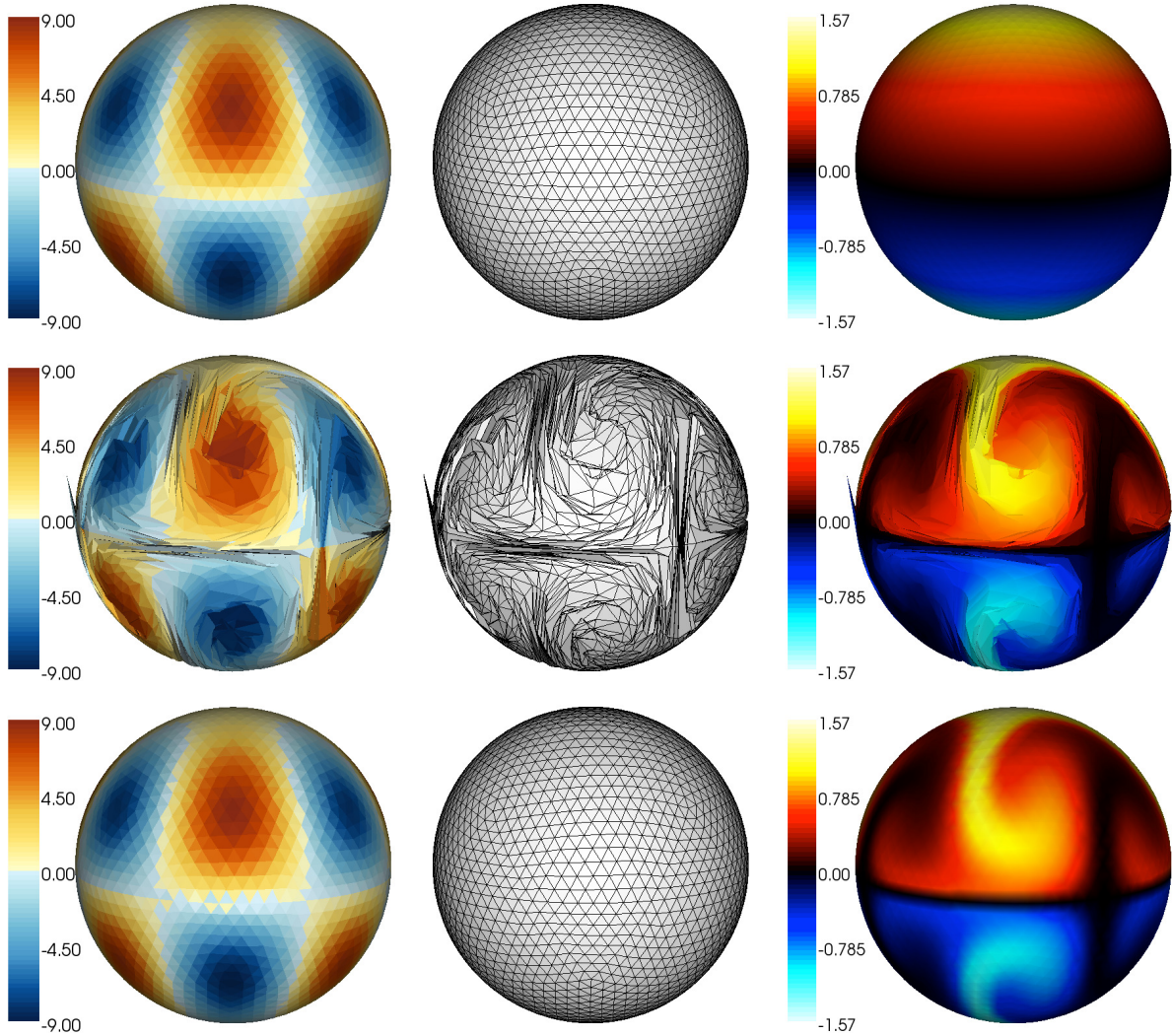


Figure 3. Example 1, Rossby-Haurwitz wave, triangular panels, $N = 5120$, time step $\Delta t = 0.01$; vorticity (left), panels (middle), passive tracer (right); $t = 0$ (top), $t = 1$ (middle, no remeshing), $t = 1$ (bottom, remeshing every 10 time steps).

6.3. Convergence under mesh refinement

Next we examine convergence of the vorticity under mesh refinement. The error in the computed vorticity at a given time t is defined by

$$e_N(t) = \left[\frac{\sum_{j=1}^N (\zeta_j - \zeta_{\text{ex}}(\mathbf{x}_j(t), t))^2 A_j}{\sum_{j=1}^N \zeta_{\text{ex}}(\mathbf{x}_j(t), t)^2 A_j} \right]^{1/2}, \quad (16)$$

where $\zeta_{\text{ex}}(\mathbf{x}, t)$ is the exact vorticity, which is known in this case. Table 1 gives the error at time $t = 1$ as a function of spatial resolution; the time step was $\Delta t = 0.005$, which ensures that the time discretization error is negligible, and remeshing was performed every 20 time steps. The first three columns give the number of triangular panels N ,

the panel angular variation $\Delta\lambda$, and the equivalent panel edge length Δs on a sphere with the Earth’s radius. The fourth column shows that the error $e_N(1)$ decreases as the mesh is refined. The fifth column gives an estimate of the convergence rate determined by two successive levels of refinement, $p = \log(e_{N/4}(1)/e_N(1))/\log 4$; the results indicate slightly faster than 2nd order convergence.

N	$\Delta\lambda$	Δs	$e_N(1)$	p
1280	8.6°	956 km	4.21e-02	—
5120	4.3°	478 km	8.35e-04	2.83
20480	2.2°	244 km	3.03e-05	2.39
81920	1.1°	122 km	1.29e-06	2.28

Table 1. Example 1, Rossby-Haurwitz wave, triangular panels, N : number of panels, $\Delta\lambda$: panel angular variation, Δs : equivalent panel edge length on a sphere with the Earth’s radius, $E_N(1)$: error in vorticity at time $t = 1$, p : estimated convergence rate, time step $\Delta t = 0.005$, remeshing every 20 time steps.

6.4. Gaussian vortex

The second example is a Gaussian vortex with initial vorticity

$$\zeta_0(\mathbf{x}) = 4\pi \exp(-16|\mathbf{x} - \mathbf{x}_c|^2) + C, \quad (17)$$

where the center \mathbf{x}_c is slightly above the equator at $(\lambda, \theta) = (0, \frac{\pi}{20})$, and the constant C is computed so that the total relative vorticity on the sphere is zero. The number of triangles is $N = 81920$ and the time step is $\Delta t = 0.005$ with remeshing every 20 time steps. Figure 4 shows the solution at $t = 0$ and $t = 3$ (three revolutions of the sphere). The vortex follows a meandering path to the northwest. At the final time, the vortex core is elliptically deformed and a thin trailing filament of negative vorticity is present. The passive tracer is entrained by the vortex and material from different latitudes is mixed in the vortex core. The trailing filament becomes thinner in time, and some checker-boarding can be seen in the vorticity at time $t = 3$, indicating a slight loss of resolution.

Since the exact vorticity is not known analytically in this case, we compared the present LPPM results with results computed by James Kent (University of Michigan) using the Lin-Rood finite-volume scheme (Lin and Rood 1996). The comparison is shown in figure 5; the Lin-Rood results were computed on a 90×180 latitude-longitude grid and the present results were interpolated from the particles to the same grid. There is good visual agreement between the two sets of results, including the wake structure behind the vortex, and this serves to further validate the present scheme.

6.5. Adaptive panel refinement

The results presented so far were computed on a Lagrangian particle/panel mesh that was essentially uniform and hence inefficient in resolving local features. Adaptive mesh

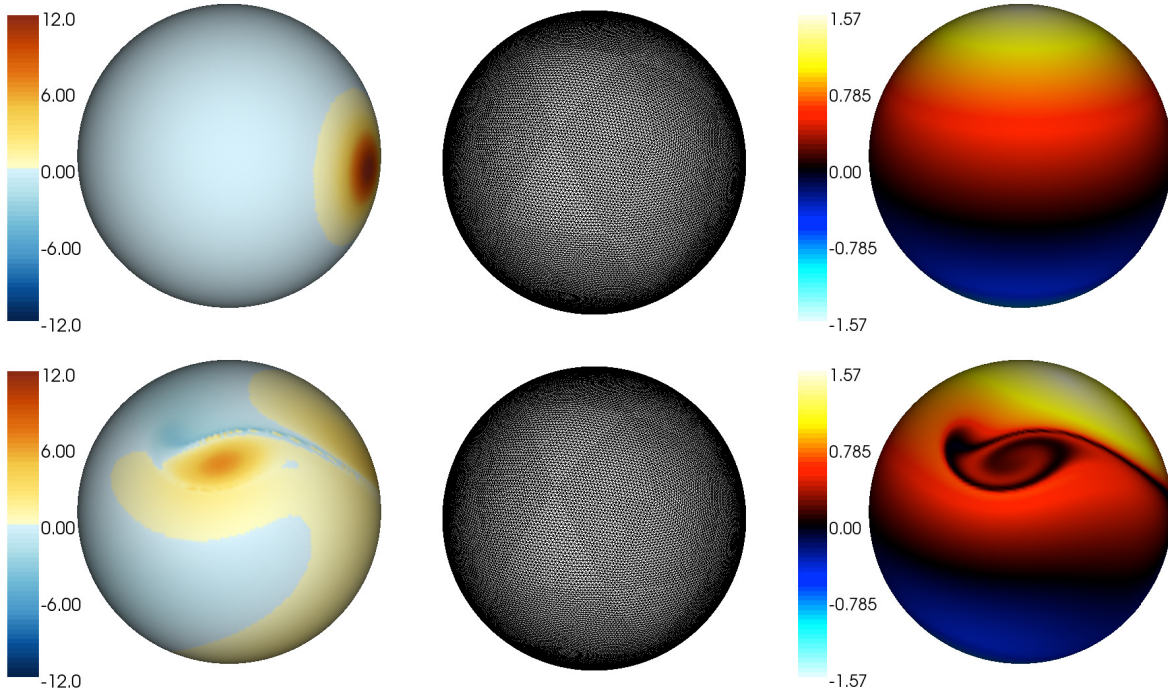


Figure 4. Example 2, Gaussian vortex, triangular panels, $N = 81920$, time step $\Delta t = 0.005$, remeshing every 20 time steps, vorticity (left), panels (middle), passive tracer (right), $t = 0$ (top), $t = 3$ (bottom).

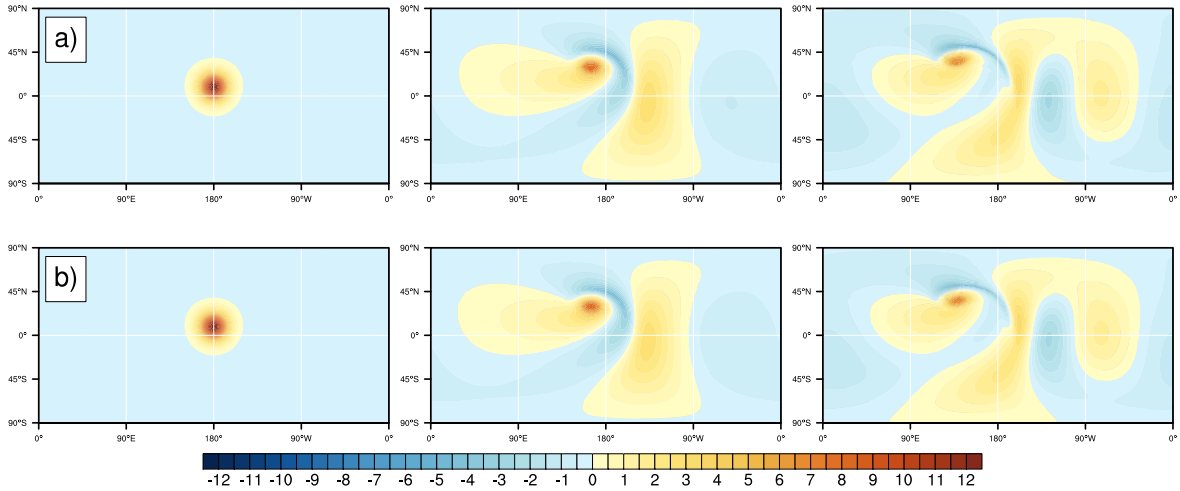


Figure 5. Example 2, Gaussian vortex, the vorticity is plotted on a latitude-longitude grid at time $t = 0, 1, 2$ (left to right), time step $\Delta t = 0.005$, (a) Lin-Rood scheme, 90×180 grid, (b) present scheme (LPPM), $N = 20480$ triangles, remeshing every 20 time steps.

refinement is a well-established approach for reducing the cost of Eulerian simulations (Behrens 2006, Jablonowski *et al* 2006), and in the present context we employ an adaptive panel refinement scheme similar to those used in vortex sheet computations (Feng *et al* 2009). Whenever a remeshing operation is performed, the code examines the

panels to determine whether any should be refined based on two criteria given below. If a panel is flagged for refinement, it is divided into four subpanels as shown in figure 6. The necessary additional particles are computed from the parent panel by cubic Hermite interpolation (Renka 1997b).

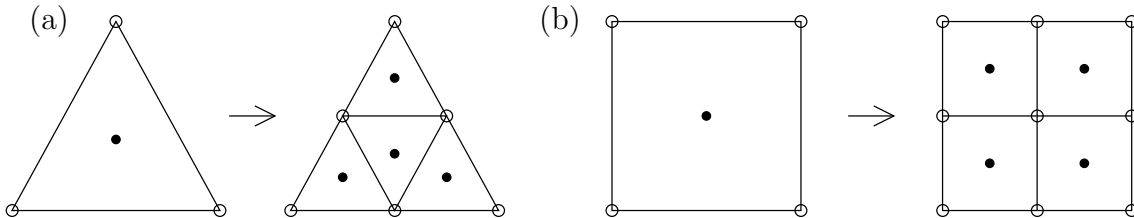


Figure 6. Adaptive panel refinement, a flagged panel is divided into four subpanels, (a) triangles, (b) quadrilaterals.

There are two refinement criteria. The first criterion is that the absolute panel circulation should be less than a given tolerance,

$$|\zeta_k|A_k < \epsilon_1, \quad (18)$$

where ζ_k is the vorticity at the panel center and A_k is the panel area. The second criterion is that the Lagrangian variation of the panel should be less than another tolerance,

$$\sum_{i=1}^3 (\max a_i^n - \min a_i^n) < \epsilon_2, \quad (19)$$

where the max and min are taken over the vertices of the remeshed panel, and a_i^n are the Cartesian coordinates of the Lagrangian parameter \mathbf{a}^n associated with a remeshed vertex.

Figure 7 shows results for the Gaussian vortex using this panel refinement scheme with tolerances $\epsilon_1 = 0.0025$, $\epsilon_2 = 0.2$, time step $\Delta t = 0.0025$, and remeshing every 20 time steps. The simulation started at $t = 0$ with $N = 6509$ triangles and finished at $t = 3$ with $N = 28319$ triangles. There were five levels of refinement; on a sphere with the Earth's radius, the largest triangle has edge length 478 km and the smallest triangle has edge length 32 km. The panels are highly refined in front of the vortex and in the thin trailing filament. The final results here are slightly better resolved than those in figure 4, despite using far fewer panels. Hence the adaptive panel refinement scheme succeeds in maintaining resolution at lower cost.

6.6. Perturbed zonal jet

The third example is a perturbed zonal jet computed using a Lagrangian cubed-sphere mesh with adaptive panel refinement and remeshing. The initial relative vorticity is

$$\zeta_0(\lambda, \theta) = 150 \sin(\theta - \theta_c(\lambda)) \exp(-300(1 - \cos(\theta - \theta_c(\lambda)))) + C, \quad (20)$$

where $\theta_c(\lambda) = \pi/4 + 0.01 \cos 12\lambda$ is the jet centerline and the constant C again ensures zero total relative vorticity. The results are shown in figure 8. The initial vorticity is

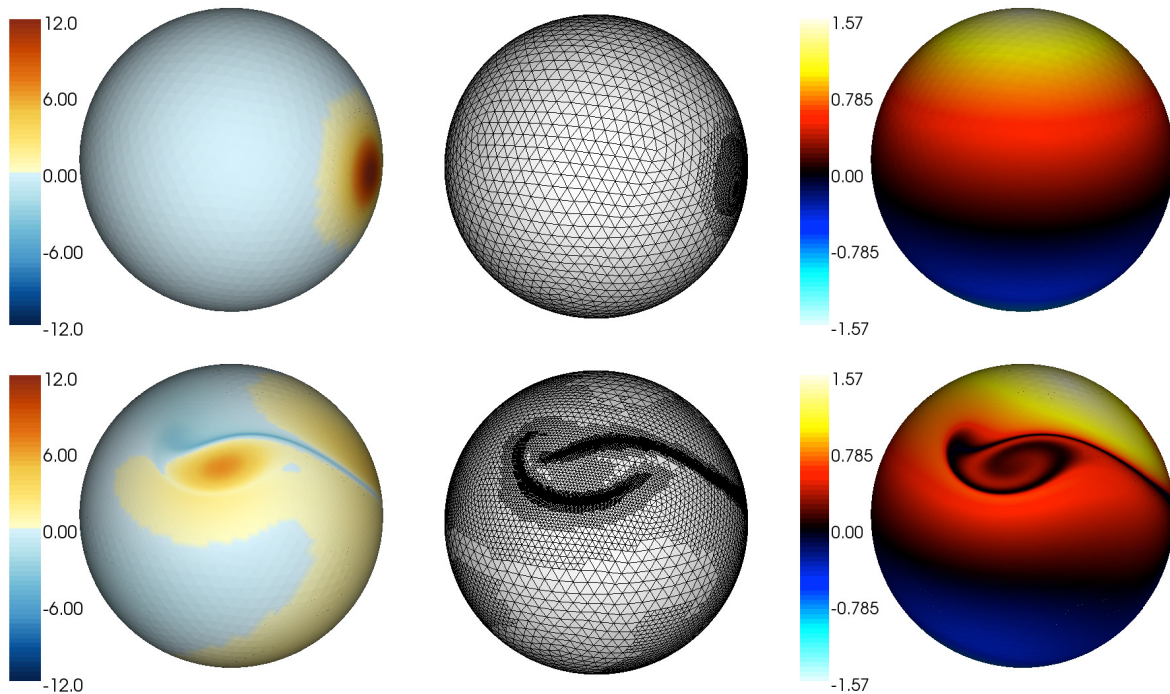


Figure 7. Example 2, Gaussian vortex, triangular panels, adaptive panel refinement with $\epsilon_1 = 0.0025, \epsilon_2 = 0.2$, time step $\Delta t = 0.005$, remeshing every 20 time steps, vorticity (left), panels (middle), passive tracer (right); $t = 0$ (top, $N = 6509$), $t = 3$ (bottom, $N = 28319$).

a thin double-layer with a small amplitude perturbation of zonal wavenumber $m = 12$. The jet rolls up into an array of counter-rotating vortices that propagate to the east. The passive tracer is entrained into the jet from both sides.

7. Discussion

As noted above, the point vortex approximation (PVA) is used to discretize the Biot-Savart integral in (12). This may seem problematic since the point vortex velocity field is singular and point vortices have chaotic dynamics (Aref 1983). Moreover, there is a large body of work using vortex-blobs, or regularized point vortices, as an alternative (Chorin 1973, Krasny 1986, Cottet and Koumoutsakos 2000). Nonetheless, finite time convergence of the PVA has been proven for smooth solutions of the Euler equations in Euclidean space (Cottet *et al* 1991, Goodman *et al* 1990, Hou and Lowengrub 1990). The present work is strictly concerned with smooth solutions and our results show that the PVA is accurate as long as the particles remain relatively well-ordered. The remeshing scheme introduces a new set of well-ordered particles at regular time intervals, and in this way we avoid the chaotic dynamics that would eventually occur with a fixed set of point vortices. Note that the present scheme has no explicit smoothing, filter, or subgrid model, but if these become necessary, e.g. in longer time simulations or more complex flow regimes, we have the option to use vortex-blobs in place of point vortices.

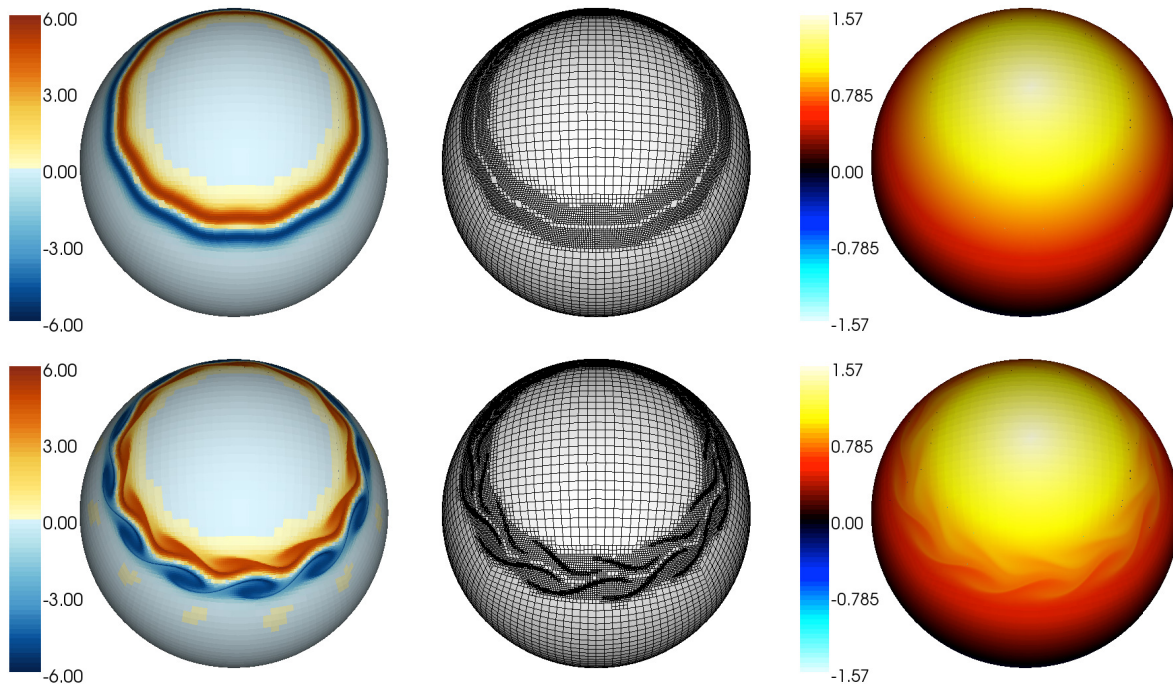


Figure 8. Example 3, perturbed zonal jet, cubed-sphere panels, adaptive panel refinement with $\epsilon_1 = 0.0008$, $\epsilon_2 = 0.16$, time step $\Delta t = 0.00125$, remeshing every 20 time steps, vorticity (left), panels (middle), passive tracer (right); $t = 0$ (top, $N = 15024$), $t = 2$ (bottom, $N = 47433$).

8. Conclusions

We presented a Lagrangian particle/panel method (LPPM) for the barotropic vorticity equations on a rotating sphere, as a first step in developing a new dynamical core for geophysical fluid flow simulations. The particles carry vorticity and the panels are used in discretizing the Biot-Savart integral for the velocity. We implemented adaptive panel refinement and a new Lagrangian remeshing scheme using inverse interpolation of the flow map. The results demonstrate the scheme’s accuracy and ability to resolve small-scale features in the vorticity and passive tracer. One feature of LPPM is that it avoids discretizing the convective derivative present in the Eulerian form of the problem. Future work will focus on the following topics.

- A treecode algorithm will be implemented to reduce the cost of evaluating the Biot-Savart integral from $O(N^2)$ to $O(N \log N)$ (Lindsay and Krasny 2001, Sakajo 2009).
- The code will be applied to study problems of geophysical interest such as the effect of sudden stratospheric warming on the stability of the polar vortex (Juckes and McIntyre 1987, Charlton and Polvani 2007).
- To further improve the code’s accuracy and efficiency, the midpoint rule will be replaced by a higher order quadrature scheme.

- A challenging goal is to extend LPPM to the shallow water equations (SWE) and apply it to benchmark test cases (Williamson *et al* 1992). Our approach will employ two Poisson equations, one for the vorticity and stream function, and another for the divergence and velocity potential function. There are also source terms involving velocity gradients to compute. Some preliminary ideas in this direction are discussed by Bosler (2013).

Acknowledgments

We thank James Kent (University of Michigan) for performing the Lin-Rood computations and the reviewers for suggestions on improving the manuscript. This work was supported by Office of Naval Research grants N00014-12-1-0509 and N00014-14-1-0075, National Science Foundation grant AGS-0723440, and the Office of Science, US Department of Energy, Award No. DE-SC0003990. The parallel computations used equipment purchased through NSF SCREMS grant DMS-1026317.

References

- Alam J M and Lin J C 2008 Toward a fully Lagrangian atmospheric modeling system *Mon. Wea. Rev.* **136** 4653–4667
- Aref H 1983 Integrable, chaotic, and turbulent vortex motion in two-dimensional flows *Annu. Rev. Fluid Mech.* **15** 345–389
- Barba L A, Leonard A and Allen C B 2005 Advances in viscous vortex methods – meshless spatial adaption based on radial basis function interpolation *Int. J. Numer. Meth. Fluids* **47** 387–421
- Behrens J 2006 *Adaptive Atmospheric Modeling (Lecture Notes in Computational Science and Engineering* vol 54) (Berlin: Springer-Verlag)
- Bogomolov V A 1977 Dynamics of vorticity at a sphere *Fluid Dyn.* **12** 863–870
- Bosler P (2013) Particle methods for geophysical flow on the sphere *PhD Thesis* University of Michigan
- Charlton A J and Polvani L M 2007 A new look at stratospheric sudden warmings. Part 1: Climatology and modeling benchmarks *J. Climate* **20** 449–469
- Chorin A J 1973 Numerical study of slightly viscous flow *J. Fluid Mech.* **57** 785–796
- Chorin A J and Marsden J E 1979 *A Mathematical Introduction to Fluid Mechanics* (New York: Springer-Verlag)
- Cottet G-H, Goodman J and Hou T Y 1991 Convergence of the grid-free point vortex method for the three-dimensional Euler equations *SIAM J. Numer. Anal.* **28** 291–307
- Cottet G-H and Koumoutsakos P D 2000 *Vortex Methods: Theory and Practice* (Cambridge: Cambridge University Press)
- Dritschel D G 1988 Contour dynamics/surgery on the sphere *J. Comput. Phys.* **78** 477–483
- Dritschel D G, Polvani L M and Mohebalhojeh A R 1999 The Contour-Adveective Semi-Lagrangian algorithm for the shallow water equations *Mon. Wea. Rev.* **127** 1551–1565
- Feng H, Kaganovskiy L and Krasny R 2009 Azimuthal instability of a vortex ring computed by a vortex sheet panel method *Fluid Dyn. Res.* **41** 051405
- Goodman J, Hou T Y and Lowengrub J 1990 Convergence of the point vortex method for the 2-D Euler equations *Commun. Pure Appl. Math.* **43** 415–430
- Hou T Y and Lowengrub 1990 Convergence of a point vortex method for 3-D Euler equations *Commun. Pure Appl. Math.* **43** 965–981
- Jablonowski C, Herzog M, Penner J E, Oehmke R C, Stout Q F, van Leer B and Powell K G 2006

- Block-structured adaptive grids on the sphere: advection experiments *Mon. Wea. Rev.* **134** 3691–3713
- Juckes M N and McIntyre M E 1987 A high-resolution one-layer model of breaking planetary waves in the stratosphere *Nature* **328** 590–596
- Kidambi R and Newton P K 1998 Motion of three point vortices on a sphere *Physica D* **116** 143–175
- Kimura Y and Okamoto H 1987 Vortex motion on a sphere *J. Phys. Soc. Japan* **56** 4203–4206
- Koumoutsakos P 1997 Inviscid axisymmetrization of an elliptical vortex *J. Comput. Phys.* **138** 821–857
- Krasny R 1986 Desingularization of periodic vortex sheet roll-up *J. Comput. Phys.* **65** 292–313
- Kropinski M C A and Nigam N 2013 Fast integral equation methods for the Laplace-Beltrami equation on the sphere *Adv. Comput. Math.* DOI 10.1007/s10444-013-9319-y
- Lin S-J and Rood R B 1996 Multidimensional flux-form semi-Lagrangian transport schemes *Mon. Wea. Rev.* **124** 2046–2070
- Lindsay K and Krasny R 2001 A particle method and adaptive treecode for vortex motion in three-dimensional flow *J. Comput. Phys.* **172** 879–907
- Newton P K 2001 *The N-Vortex Problem: Analytical Techniques* (New York: Springer-Verlag)
- Perlman M 1985 On the accuracy of vortex methods *J. Comput. Phys.* **59** 200–223
- Renka R 1997a Algorithm 772: STRIPACK: Delaunay triangulation and Voronoi diagram on the surface of a sphere *ACM Trans. Math. Software* **23** 416–434
- Renka R 1997b Algorithm 773: SSRFPACK: Interpolation of scattered data on the surface of a sphere with a surface under tension. *ACM Trans. Math. Software* **23** 435–442
- Russo G and Strain J A 1994 Fast triangulated vortex methods for the 2D Euler equations *J. Comput. Phys.* **111** 291–323
- Sakajo T 2009 An extension of Draghicescu’s fast tree-code algorithm to the vortex method on a sphere *J. Comput. Appl. Math.* **225** 158–171
- Surana A and Crowdy D 2008 Vortex dynamics in complex domains on a spherical surface *J. Comput. Phys.* **227** 6058–6070
- Taylor M A and Fournier A 2010 A compatible and conservative spectral element method on unstructured grids *J. Comput. Phys.* **229** 5879–5895
- Vallis G K 2006 *Atmospheric and Oceanic Fluid Dynamics* (Cambridge: Cambridge University Press)
- Wang L 2010 Radial basis functions and vortex methods and their application to vortex dynamics on a rotating sphere *PhD Thesis* University of Michigan
- Williamson D L, Drake J B, Hack J J, Jakob R and Swarztrauber P N 1992 A standard test set for numerical approximations to the shallow water equations in spherical geometries *J. Comput. Phys.* **102** 211–224